A robust method for performance evaluation of the vapor cell for magnetometry

Zhi Liu(柳治)[1,2], Sheng Zou(邹升)[1,2], Kaifeng Yin(尹凯峰)[1,2], Tao Shi(石韬)[1,2], Junjian Tang(唐钧剑)[1,2], and Heng Yuan(袁珩)[1,2,†]

[1] *School of Instrumentation Science and Optoelectronics Engineering, Beihang University, Beijing* 100191, *China*
[2] *Hangzhou Innovation Institute of Beihang University, Hangzhou* 310051, *China*

(Received 6 September 2022; revised manuscript received 14 November 2022; accepted manuscript online 29 November 2022)

A robust performance evaluation method for vapor cells used in magnetometers is proposed in this work. The performance of the vapor cell determines the sensitivity of the magnetic measurement, which is the core parameter of a magnetometer. After establishing the relationship between intrinsic sensitivity and the total relaxation rate, the total relaxation rate of the vapor cell can be obtained to represent the intrinsic sensitivity of the magnetometer by fitting the parameters of the magnetic resonance experiments. The method for measurement of the total relaxation rate based on the magnetic resonance experiment proposed in this work is robust and insensitive to ambient noise. Experiments show that, compared with conventional sensitivity measurement, the total relaxation rate affected by magnetic noise below 0.9 nT, pump light frequency noise below 1.5 GHz, pump light power noise below 9%, probe light power noise below 3% and temperature fluctuation of 150 ± 3 °C deviates by less than 2% from the noise-free situation. This robust performance evaluation method for vapor cells is conducive to the construction of a multi-channel high-spatial-resolution cardio-encephalography system.

Keywords: evaluation method, magnetometer, robust, vapor cell

PACS: 07.07.Df, 07.55.Ge, 07.55.–w, 33.35.+r **DOI:** 10.1088/1674-1056/aca6d5

1. Introduction

Ultrasensitive magnetic measurement based on quantum phenomena has found numerous applications, such as magnetic target localization, current sensing, magnetocardiography (MCG), and magnetoencephalography (MEG).[1–4] A state of the art spin-exchange relaxation-free (SERF) magnetometer can achieve the best fundamental sensitivity with the advantage of a flexible configuration and low cost, making it the most promising technology in this field.[5–7] The core component of a SERF magnetometer is an atomic vapor cell containing an alkali metal and buffer gas;[8,9] its performance determines the sensitivity of the magnetic measurement.[10,11]

Artificial operations during the fabrication process affect the components of the vapor cells, resulting in inconsistent parameters in the same batch.[12,13] The vapor cell and other components that make up a miniaturized magnetometer are rigidly connected and cannot be disassembled without damage. Therefore, it is necessary to evaluate the performance of the vapor cell before assembling the magnetometer. For example, Perry *et al.* evaluated the red detuning of more than 60 cells to select similar ones for assembly.[14] Wang *et al.* optimized the gas pressure of a Rb vapor cell through an experiment measuring sensitivity, which is the conventional evaluation method for vapor cells.[15,16] However, there is a lack of research on the robustness of vapor cell evaluation methods. The conventional method for evaluating sensitivity requires high system stability and low environmental noise. When there is a considerable magnetic noise due to a poor magnetic shielding effect,[17,18] or the frequency and power of the laser beam are unstable,[19,20] or the system has temperature fluctuations,[21,22] the experimental sensitivity is dominated by external noise and cannot represent the performance of the vapor cell. Therefore, it is of great significance to find a more robust method for evaluating vapor cells.

We propose a robust performance evaluation method for vapor cells used in magnetometers. After establishing the relationship between the total relaxation rate $R_{\rm tot}$ and the intrinsic sensitivity, the total relaxation rate $R_{\rm tot}$ of the vapor cell can be obtained by fitting the parameters of the magnetic resonance experiment to evaluate the performance of the vapor cell.[23,24] This method can operate reliably under unstable factors such as magnetic noise, optical frequency noise, optical power noise and temperature fluctuations.

2. Theoretical principles

The sensitivity of a magnetometer can be defined through $\delta B = B_{\rm cal}/{\rm SNR}$,[25] where SNR is the signal-to-noise ratio, $B_{\rm cal}$ is the calibration magnetic field, which is a fixed value, and δB is the sensitivity. There are two main sources of noise. The first is magnetic noise, $N_{\rm mag}$, that still exists when the magnetometer is not operating, such as magnetic noise from nearby metals. This noise can be theoretically calculated with the Johnson-current-induced noise formula. The second is probe noise, $N_{\rm probe}$, which contains the spin-projection noise,

†Corresponding author. E-mail: hengyuan@buaa.edu.cn
© 2023 Chinese Physical Society and IOP Publishing Ltd

photon-shot noise and technical noise. This noise remains almost the same for different vapor cells. The noise strength in the SNR can be expressed by $N_{\rm all}=\sqrt{N_{\rm mag}^2+N_{\rm probe}^2}$, which can be regarded as approximately invariant. Therefore, the sensitivity of the magnetometer is inversely proportional to the signal strength.

The signal strength of the magnetometer can be obtained by solving the Bloch equation,[26,27] which is simplified from the density matrix equation[28]

$$\frac{\mathrm{d}}{\mathrm{d}t}\boldsymbol{S}=\frac{1}{q(P)}\left[\gamma_{\rm e}\boldsymbol{B}\times\boldsymbol{S}+R_{\rm op}\left(\frac{1}{2}\boldsymbol{s}-\boldsymbol{S}\right)-R_{\rm rel}\boldsymbol{S}\right], \quad (1)$$

where $q(P)$ is the slowing-down factor which is related to atom spin polarization P, $\gamma_{\rm e}=2\pi\times 2.8$ MHz·G^{-1} is the electron gyromagnetic ratio, $\boldsymbol{B}$ is the applied magnetic field, $R_{\rm op}$ is the optical pumping rate, $\boldsymbol{s}$ is the optical pumping vector, whose magnitude is the degree of circular polarization of the pump light and whose direction is the same as the pump light, and $R_{\rm rel}$ is the relaxation rate which contains the spin exchange relaxation rate $R_{\rm ser}$, spin destruction relaxation rate $R_{\rm sd}$, wall collision relaxation rate $R_{\rm wall}$ and the relaxation rate due to the probe light $R_{\rm pr}$.

Assuming that the circularly polarized pump light propagates along the x-axis, the linearly polarized probe light propagates along the z-axis and the magnetic field to be measured is along the y-axis, the response to the calibration magnetic field B_y is

$$S_z=\frac{\gamma_{\rm e}R_{\rm op}B_y}{2(R_{\rm op}+R_{\rm rel})^2}. \quad (2)$$

The response information can be extracted from the optical rotation angle θ through the balanced polarimetry technique.[29] Truncating the Taylor series expansion of the result appropriately, we can get

$$I_1-I_2=I_0\sin(2\theta)\approx 2I_0\theta, \quad (3)$$

where I_1 and I_2 are the light intensity of the two output detection beams with different polarization directions and

$$\theta=\frac{1}{2}f_{\rm D2}lr_{\rm e}cnS_z\frac{1}{\nu-\nu_{\rm D2}}, \quad (4)$$

where $f_{\rm D2}=0.668$ is the oscillator strength of the rubidium D2 line, $l=3$ mm is the inner diameter of the vapor cell, $r_{\rm e}=2.82\times10^{-15}$ m is the classical electron radius, $c=299792458$ m·s^{-1} is the speed of light, $n=1.01\times10^{20}$ m^{-3} is the rubidium saturated vapor density at 150 °C, ν is the probe light frequency and $\nu_{\rm D2}$ is the rubidium D2 line frequency.

Assuming that the conversion coefficient from optical power to voltage is G, the output signal strength U can be obtained by combining Eqs. (2)–(4) as

$$U=\frac{1}{2}GI_0lr_{\rm e}cnf_{\rm D2}\frac{1}{\nu-\nu_{\rm D2}}\frac{\gamma_{\rm e}R_{\rm op}B_y}{(R_{\rm op}+R_{\rm rel})^2}. \quad (5)$$

Since the probe light deviates from the rubidium D2 line over 100 GHz in our experiment, the difference caused by $(\nu-\nu_{\rm D2})$ can be ignored for different vapor cells. With the pump light intensity unchanged, which means that $R_{\rm op}$ is approximately the same for different vapor cells, we can conclude that the magnetometer sensitivity is proportional to the square of the total relaxation rate

$$\mathrm{SEN}=\frac{2B_{\rm cal}N_{\rm all}R_{\rm tot}^2}{GI_0lr_{\rm e}cnf_{\rm D2}\gamma_{\rm e}R_{\rm op}B_y}, \quad (6)$$

where $R_{\rm tot}=R_{\rm rel}+R_{\rm op}$. Thus, the relationship between the magnetometer sensitivity and the total relaxation rate is established.

In the magnetic resonance experiment, the bias magnetic field B_0 is applied on the x-axis and the oscillating field $B_y=B'\cos(\omega t)$ is applied on the y-axis. Assuming that $\tilde{S}=S_z+\mathrm{i}S_y$, $\tilde{B}=B_z+\mathrm{i}B_y$, we can get the following equation from Eq. (1):

$$\frac{\mathrm{d}}{\mathrm{d}t}\tilde{S}+\left(\frac{1}{T_2}+\mathrm{i}\omega_0\right)\tilde{S}=\mathrm{i}\gamma S_0\tilde{B}, \quad (7)$$

where $\Delta\omega=\frac{1}{T_2}=\frac{R_{\rm op}+R_{\rm rel}}{q(P)}$,[30] $\omega_0=\gamma B_0$, $\gamma=\frac{\gamma_{\rm e}}{q(P)}$, and $S_0=\frac{R_{\rm op}}{2(R_{\rm op}+R_{\rm rel})}$. Ignoring the oscillation attenuation term, we can solve the steady state of Eq. (7) to get

$$\begin{aligned}S_z&=\mathrm{Re}[\tilde{S}]=-\frac{\gamma S_0B'}{2}[M+N],\\ M&=\frac{\Delta\omega\cos(\omega t)+(\omega+\omega_0)\sin(\omega t)}{\Delta\omega^2+(\omega+\omega_0)^2},\\ N&=\frac{\Delta\omega\cos(\omega t)-(\omega_0-\omega)\sin(\omega t)}{\Delta\omega^2+(\omega_0-\omega)^2}.\end{aligned} \quad (8)$$

This result can be demodulated in the lock-in amplifier to obtain the in-phase term, which is the Lorentzian absorption type, and the out-of-phase term, which is the Lorentzian dispersion type. Synthesizing the two parts, the output signal is

$$\gamma S_0B'\sqrt{\frac{\Delta\omega^2+\omega^2}{[\Delta\omega^2+(\omega+\omega_0)^2][\Delta\omega^2+(\omega-\omega_0)^2]}}. \quad (9)$$

By fitting the experimental results, we can obtain ω_0 and $\Delta\omega$ and then calculate $R_{\rm tot}=R_{\rm op}+R_{\rm rel}=\Delta\omega\gamma_{\rm e}B_0/\omega_0$. By fitting the relationship between the total relaxation rate and the bias magnetic field with a quadratic function, the zero-field total relaxation rate can be obtained.[31,32]

3. Experimental setup

The system for sensitivity measurement and the magnetic resonance experiments is shown in Fig. 1. The pump laser and the probe laser entered the prototype through the fiber. The fiber ports contained collimating lenses to ensure that the outgoing laser beams were parallel beams with a diameter of 2.7 mm. The wavelength of the pump laser was set as the absorption peak of different vapor cells, and the wavelength of

the probe laser was set as 780.020 nm. The pump laser passed through the linear polarizer and quarter-wave plate to become circularly polarized. Then the pump laser was reflected by the reflecting mirror to travel along the x-axis through the vapor cell. The probe laser passed through the linear polarizer and half-wave plate to become linearly polarized. The probe laser then traveled through the vapor cell along the z-axis and was split by the lateral displacement polarized beam splitter into a P beam and an S beam. Afterward, the probe light was detected by the difference photodiode and converted into a voltage signal through the transimpedance amplifier (TIA). After that, the signal was filtered by a 10 kHz low-pass filter to avoid the influence of the heating current. The vapor cell was put into a boron nitride oven and its temperature was stabilized in the range of 150 ± 0.02 °C through closed-loop control. The wave generator generated DC signals to realize magnetic field compensation through the coils. The wavelength was tested by a wavelength meter with a sampling frequency of 500 Hz and absolute accuracy of 60 MHz.

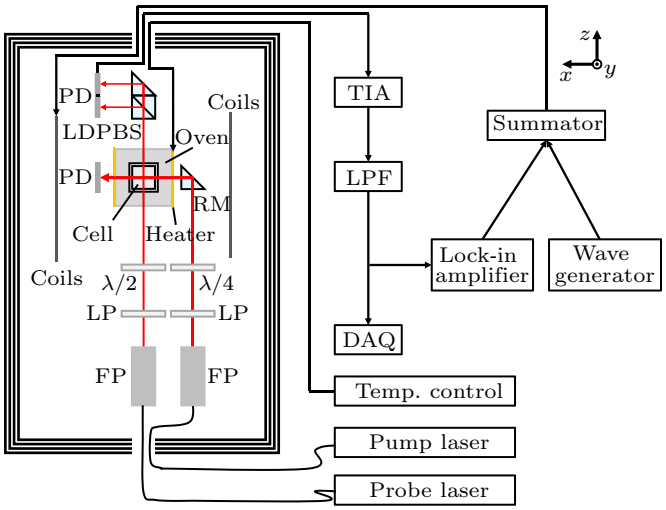


Fig. 1. Schematic diagram of the experimental system (FP, fiber port; LP, linear polarizer; $\lambda/4$ and $\lambda/2$, quarter-wave and half-wave plates, respectively; RM, reflecting mirror; PD, photodiode; LDPBS, lateral displacement polarized beam splitter; TIA, transimpedance amplifier; LPF, low-pass filter; DAQ, data acquisition).

The inner wall of the cell was 3 mm × 3 mm × 3 mm and there was a droplet of ^{87}Rb and nitrogen between 0.4 amg and 2.7 amg in the cell (1 amg is defined as the number density of an ideal gas at standard temperature and pressure). In the sensitivity calibration experiment, the pump light power was set to 100 μW and the probe light power was set to 250 μW. The signal passing through the low-pass filter was collected directly for power spectral density analysis to obtain the sensitivity. In the magnetic resonance experiment, the pump light power was set to 20 μW and the probe light power was set to 100 μW. The lock-in amplifier generated a 1 nT peak frequency sweep modulation voltage on the coils. The signal passing through the low-pass filter was demodulated by the lock-in amplifier. The bias magnetic field was changed in steps of 4.446 nT, and 14 sets of different bias magnetic fields were scanned. Each sweep curve changed from 10 Hz to 350 Hz, 200 sampling points were taken and each point was tested for 0.5 s for averaging.

In the following experiments, magnetic noise, optical frequency noise and optical intensity noise were applied to the magnetometer. Among these, magnetic noise was generated by applying the voltage noise from the signal generator to the coils, as shown in Fig. 2(a). As for optical frequency noise, because the pump laser was generated by an external cavity semiconductor laser whose frequency was controlled by the piezoelectric ceramics, different amplitudes of voltage noise were applied to the ceramics to generate different optical frequency noises, as shown in Fig. 2(b). Additionally, since the pump light and probe light entered the magnetometer through the fiber, an acousto-optic modulator (AOM) was introduced at the fiber interface. By controlling its input voltage, the light power noise was realized, as shown in Fig. 2(c). The above three types of noise were rooted in the voltage noise generated by the signal generator, which is Gaussian noise, and we set its frequency band as 0 Hz–200 Hz.

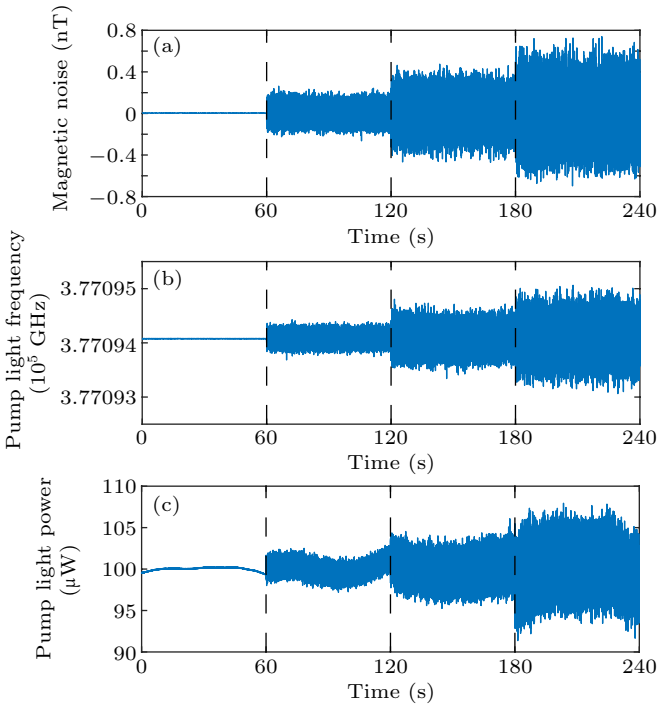


Fig. 2. (a) Magnetic noise. The four parts in the figure relate to 0 nT, 0.3 nT, 0.6 nT, and 0.9 nT noise, respectively. (b) Optical frequency noise. The four parts in the figure relate to 0 GHz, 0.5 GHz, 1 GHz, and 1.5 GHz noise, respectively. (c) Optical power noise. The four parts in the figure relate to 0%, 3%, 6%, and 9% noise, respectively.

4. Results and discussion

The theoretical foundation of this method is that the probe noise of the magnetometer remains constant with different vapor cell parameters, which can be obtained through experi-

ments. The pump light is turned off in the pump–probe configuration magnetometer, and the acquired signal is the probe noise alone. Figure 3 shows the results for probe noise measurement with different nitrogen pressures, which fluctuate between 5.6×10^{-5} V·Hz$^{-1/2}$ and 6.2×10^{-5} V·Hz$^{-1/2}$. In addition, among the components of the total relaxation rate $R_{\rm tot}$, the differences in the pump light term $R_{\rm op}$ and the probe light term $R_{\rm pr}$ are of the order of a few Hertz for different vapor cells on the condition that the pump and probe light power remains unchanged. Besides, the spin exchange relaxation rate $R_{\rm ser}$ is mainly related to the magnetic field, which does not need to be considered in the zero-field total relaxation rate obtained after the quadratic fitting. In addition to the above relaxation terms, the total relaxation rate only comprises the cell-related relaxation rate $R_{\rm cell}$, which contains the spin destruction relaxation rate $R_{\rm sd}$ and the wall collision relaxation rate $R_{\rm wall}$. This term, which is about several hundreds of Hertz, is related to the vapor cell parameters. Therefore, $R_{\rm tot}$ can represent the performance of the vapor cell.

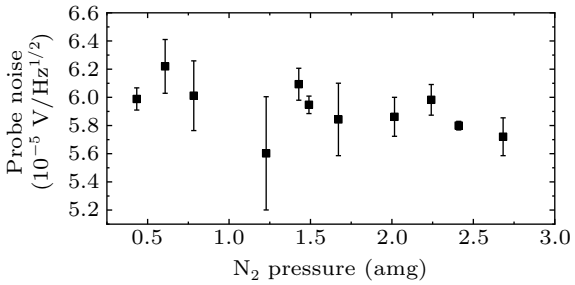


Fig. 3. The results of probe noise measurement for different nitrogen pressure vapor cells.

The sensitivity and total relaxation rate under different nitrogen pressures are shown in Fig. 4(a). The nitrogen pressure was tested through the light absorption method below 120 °C.[33,34] The trends of sensitivity and total relaxation rate are almost the same. They are relatively poor in the lower and higher nitrogen pressure sections, and the optimum value is reached at around 1.13 amg. Theoretical analysis shows that when the nitrogen pressure is low, the alkali metal atoms are more likely to collide with the cell wall, resulting in the loss of spin directivity. In contrast, when the nitrogen pressure is high, the alkali metal atoms will have more collisions with the buffer gas, causing spin destruction. Therefore, there is a trade-off value of nitrogen pressure that minimizes the total relaxation rate and optimizes the sensitivity. Wang *et al.*[15] concluded that the N_2 optimal pressure is 1.2 amg–2.2 amg under different pump light intensities, which is close to our experimental results. The relationship between sensitivity SEN and nitrogen pressure P can be expressed by $\mathrm{SEN}=4.0596P+5.2054/P$, whose R^2 is 0.9327. Similarly, the total relaxation rate can also be related to the nitrogen pressure, $R^2_{\rm rel}=7919.8P+10092/P$, whose R^2 is 0.8505. We reprocessed the data in Fig. 4(a). Using $R^2_{\rm rel}$ as the horizontal axis and sensitivity as the vertical axis, the correlation between the two parameters is highlighted in Fig. 4(b). The fitting relation can be expressed by $\mathrm{SEN}=4.0519+3.1786\times10^{-4}R^2_{\rm tot}$, whose R^2 is 0.8086. Therefore, the relationship between the total relaxation rate $R_{\rm tot}$ and the intrinsic sensitivity is obtained.

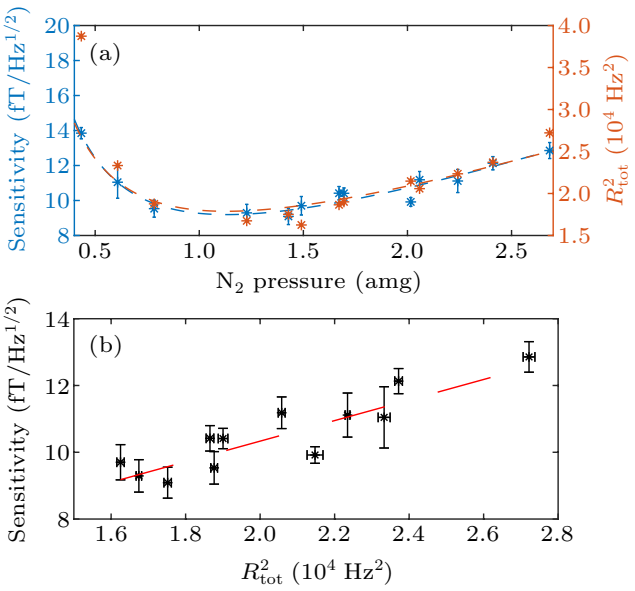


Fig. 4. (a) The results of sensitivity and total relaxation rate measurement for different nitrogen pressure vapor cells. The blue dots and line represent the sensitivity, and the red dots and line represent the square of the total relaxation rate. (b) The relationship between the square of the total relaxation rate and the sensitivity. The vertical error bar represents the results of five sensitivity measurements, and the horizontal error bar represents the results of nine relaxation rate measurements.

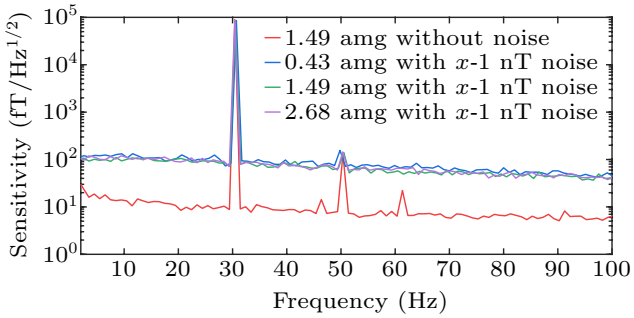


Fig. 5. The sensitivity of different nitrogen pressure cells with 1 nT magnetic noise whose bandwidth is 200 Hz along the x-axis.

When there is disturbance from external noise, the intrinsic sensitivity of the cells with different nitrogen pressures is covered by the noise, which makes sensitivity measurement to characterize the performance of the cell impossible. Taking the application of 1 nT magnetic noise whose bandwidth is 200 Hz on the x-axis as an example, the test results for different nitrogen pressure cells are shown in Fig. 5. The sensitivity results for vapor cells containing 0.43 amg, 1.49 amg, and 2.68 amg nitrogen under the 1 nT noise are 82.32 fT·Hz$^{-1/2}$, 84.08 fT·Hz$^{-1/2}$, and 89.28 fT·Hz$^{-1/2}$, respectively. The experimental sensitivity of the magnetometer contains the intrinsic sensitivity of the vapor cell and the external noise interfer-

ence, which prevents effective evaluation of the performance of the vapor cell. On the contrary, the total relaxation rate $R_{\rm tot}$ is obtained by fitting thousands of data points, so the magnetic resonance method is more robust for characterizing the performance of the vapor cell and its ability to overcome noise disturbance is more potent.

Sensitivity measurements and magnetic resonance experiments were carried out under different noises. The noise sources for the magnetometer include the magnetic noise in different directions, the frequency and power noises of the pump light, the frequency and power noises of the probe light and the temperature fluctuations of the vapor cell. Among these, the probe light frequency deviates far from the resonance center so its influence can be ignored. The following experiments were carried out with a vapor cell containing 1.49 amg nitrogen, whose pump light absorption peak is 795.00708 nm under 150 °C.

First, experiments related to magnetic noise were carried out. Magnetic noises with a bandwidth of 200 Hz and amplitudes of 0.3 nT, 0.6 nT, and 0.9 nT were applied on the *x*-, *y*-, and *z*-axis, respectively. The sensitivity measurement results with 0.9 nT noise are shown in Fig. 6(a). The sensitivity deteriorates rapidly in the presence of magnetic noise, especially on the *y*-axis. Noise affects the *z*-axis more severely than the *x*-axis, as shown in Fig. 6(c). The effect of noise on sensitivity is proportional to the noise amplitude, consistent with the previous analysis of the signal-to-noise ratio. The sweep curves with 0.9 nT noise are shown in Fig. 6(b). Only the magnetic resonance curves with bias magnetic fields of 17.78 nT, 31.12 nT, and 44.46 nT are shown. The effect of noise can be seen from the random fluctuation of the curve. This effect can be characterized by the parameter C-RMSE, shown in Table 1. C-RMSE is obtained by calculating the square sum of the root mean square error (RMSE) in the fitting process of a set of magnetic resonance experimental curves and taking the square root. The larger the C-RMSE, the more the fitted curve is affected by noise. The noise of the same amplitude has the most serious impact on the *y*-axis, followed by the *z*-axis, with the *x*-axis being almost unaffected. The pump light is along the *x*-axis and the probe light is along the *z*-axis, making the rubidium atoms inherently more sensitive to the magnetic field on the *y*-axis. When the bias magnetic field along the *x*-axis gradually increases beyond 10 nT, the noise below 1 nT can be ignored, causing the *x*-axis noise situation to be the closest to the noise-free situation. Figure 6(d) shows the test results for the total relaxation rate under different noise conditions. Taking the measurement result with no external noise at 150 °C as the standard, which is 127.46 Hz, the deviations of noise below the 0.9 nT measurement results are characterized by the relative error (RE) in Table 1 and are all within ±0.6%.

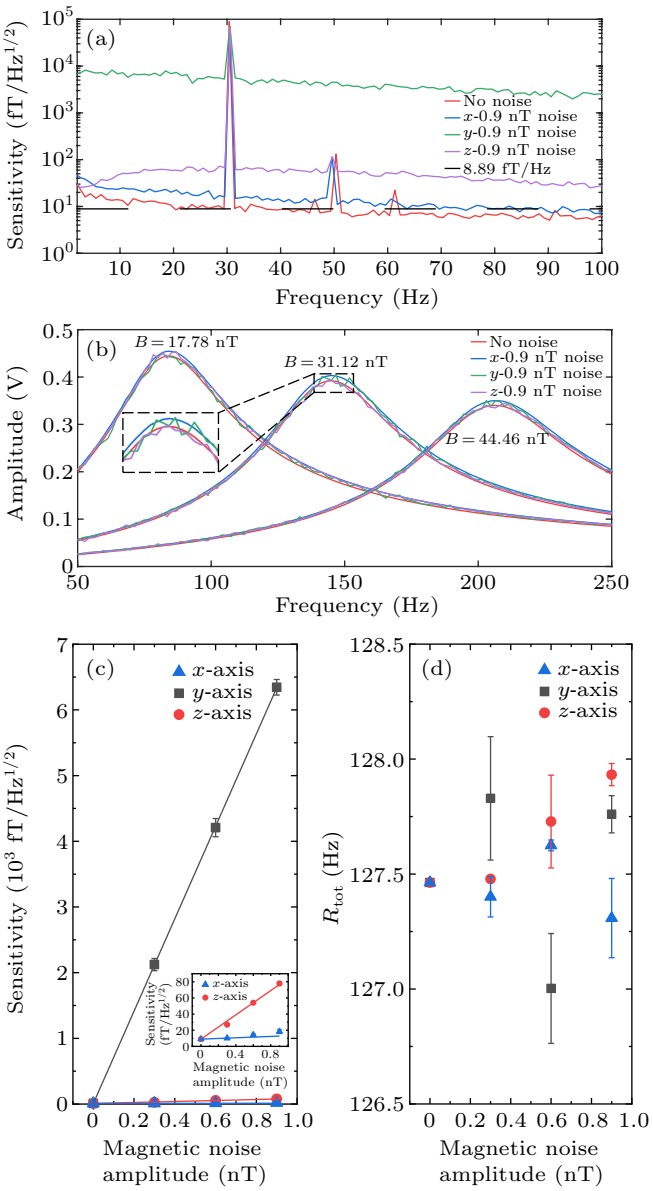


Fig. 6. (a) The sensitivity measurement results with 0.9 nT 200 Hz noise on the *x*-, *y*-, and *z*-axis. The red line is the sensitivity measurement result without noise, and the noise floor is shown as the black dotted line. (b) The magnetic resonance curves with 0.9 nT 200 Hz noise on the *x*-, *y*-, and *z*-axis. The red line is the magnetic resonance curve without noise. (c) Sensitivity measurement results under different noise conditions. Every error bar represents the results of three measurements. (d) The total relaxation rate measurement results under different noise conditions. Every error bar represents the results of three measurements.

In addition to magnetic field noise, the stability of light is also an important factor affecting vapor cell evaluation. Figure 7(a) shows the sensitivity results corresponding to different pump light frequency noises with a bandwidth of 200 Hz and figure 7(b) shows the sensitivity results corresponding to different pump light and probe light power noises with a bandwidth of 200 Hz. The light power noise of the same magnitude has a much more significant influence on the probe light than the pump light. Similar to the results for magnetic noise, the sensitivity is proportional to the noise amplitude. The influences of optical frequency and power noise on the total relaxation rate are shown in Figs. 7(c) and 7(d). The effects

of noise on the magnetic resonance curves are shown in Table 1 through C-RMSE. The influence of the frequency noise on the magnetic resonance curve is almost negligible. The influence of the probe light power noise is more significant than the pump light power noise, but is still of the same order of magnitude. Again, taking the measurement result with no external noise as the standard, the deviations of pump light frequency noise measurements below the 1.5 GHz condition are all within ±0.2%, the deviations of pump light power noise below the 9% condition are all within ±0.7% and the deviations of probe light power noise below the 3% condition are all within ±0.7%, as shown in Table 1. The above results reflect the high robustness and anti-noise characteristics of the magnetic resonance method.

Table 1. Influence of different noises on magnetic resonance experiments.

Noise	R_{tot} (Hz)	RE	C-RMSE	Noise	R_{tot} (Hz)	RE	C-RMSE
No noise	127.49	0.00%	2.59×10^{-3}				
y-0.3 nT	127.83	0.27%	4.72×10^{-3}	0.5 GHz	127.47	−0.01%	2.85×10^{-3}
y-0.6 nT	127.00	−0.38%	7.00×10^{-3}	1 GHz	127.55	0.05%	2.80×10^{-3}
y-0.9 nT	127.76	0.22%	9.87×10^{-3}	1.5 GHz	127.42	−0.05%	2.71×10^{-3}
z-0.3 nT	127.48	−0.01%	3.74×10^{-3}	pump 3%	127.77	0.22%	2.96×10^{-3}
z-0.6 nT	127.73	0.19%	5.66×10^{-3}	pump 6%	127.41	−0.06%	4.17×10^{-3}
z-0.9 nT	127.93	0.35%	7.46×10^{-3}	pump 9%	126.83	−0.51%	4.00×10^{-3}
x-0.3 nT	127.40	−0.07%	3.05×10^{-3}	probe 1%	127.42	−0.05%	3.15×10^{-3}
x-0.6 nT	127.62	0.11%	2.78×10^{-3}	probe 2%	127.94	0.35%	4.04×10^{-3}
x-0.9 nT	127.31	−0.14%	2.64×10^{-3}	probe 3%	127.83	0.27%	9.26×10^{-3}

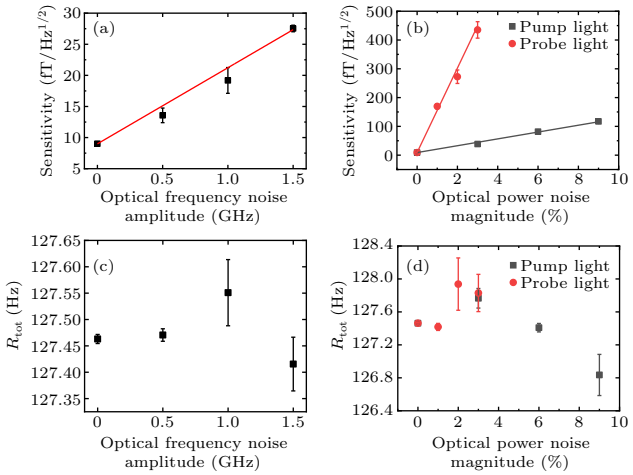


Fig. 7. (a) and (b) The sensitivity results corresponding to different pump light frequency noises, different pump light power noises and different probe light power noises with a bandwidth of 200 Hz. (c) and (d) The total relaxation rate results corresponding to different pump light frequency noises, different pump light power noises and different probe light power noises with a bandwidth of 200 Hz. Every error bar in the four figures represents the results of three measurements.

Another critical factor affecting vapor cell evaluation is the temperature. The temperature difference between the inside of the vapor cell and the Pt resistance measurement point will cause systematic errors. It takes a long time for the temperature to stabilize, leading to significant random errors. We tested R_{tot} at different stable temperatures, and marked the error of R_{tot} relative to 150 °C on the right axis, as shown in Fig. 8. The experiment indicates that within the temperature range 150 ± 3 °C, the error in R_{tot} is less than 2%. In contrast, the number density of alkali metal atoms at 147 °C is 8.69×10^{19} m^{-3}. The corresponding response signal will deteriorate by 13.92%. The above results characterize the stability of the total relaxation rate measurement results relative to the sensitivity.

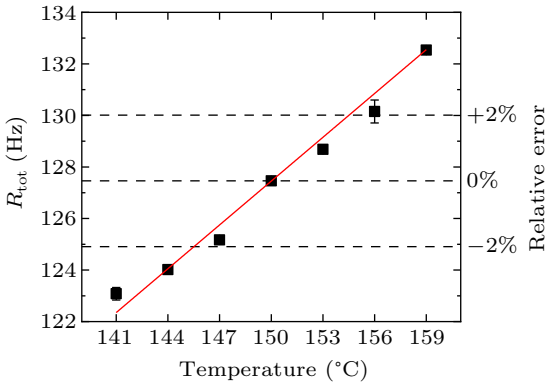


Fig. 8. The total relaxation rate under different temperatures. The right axis is the relative error with the 150 °C result as the standard. Every error bar represents the results of three measurements.

In essence, the sensitivity evaluation standard relies on power spectral density analysis. As the spectral measurement monitors the power per bandwidth, the sensitivity measurement effectively measures the power influence of the zero-mean noise source. Therefore, the noise sources with zero-mean average over periods, for example, of tens of milliseconds, have a non-negligible impact on sensitivity. In contrast, each acquisition point of the magnetic resonance curve has been averaged for 0.5 s. The nonlinear least squares method is used in sweep curve fitting and total relaxation rate fitting, which also has the function of eliminating or reducing noise. Therefore, the total relaxation rate measurement method based on the magnetic resonance experiment proposed in this work is more robust and insensitive to ambient noise. The non-zero-mean noise can be seen as an offset plus the zero-mean noise. The biased magnetic field has a severe impact on sensitivity. For example, the dynamic range of the commercial atomic magnetometer QuSpin is ±1.5 nT, beyond which the signal intensity will deviate from the linear region. However, mag-

netic fields of several nT have a negligible influence on the bias magnetic field, which is beyond 10 nT in the magnetic resonance measurement. Therefore, from the perspective of non-zero-mean magnetic noise, the magnetic resonance method is more resistant to noise. In addition, the effect of pump light power and probe light power on the total relaxation rate is measured. Fitting the total relaxation rate under different optical power, we get $R_{\rm tot} = 0.0386 \times P_{\rm probe}\ (\mu{\rm W}) + 0.5949 \times P_{\rm pump}\ (\mu{\rm W}) + 111.73$. This formula shows that changes in the pump light power and probe light power of the order of μW have little effect on the total relaxation rate, which also represents that the magnetic resonance method still has good resistance to the non-zero mean optical noise.

5. Conclusion and perspectives

In conclusion, the theoretical connection between magnetometer sensitivity and the total relaxation rate of a vapor cell is established, and the measurement methods are given. Experiments show that this magnetic resonance method can obtain the relaxation parameters and further predict the intrinsic sensitivity of a vapor cell. Different noises with a bandwidth of 200 Hz were carried investigated. The effect of magnetic noise below 0.9 nT under different axes, pump light frequency noise below 1.5 GHz, pump light power noise below 9%, and probe light power noise below 3% on the total relaxation rate is less than ±0.7%, and the corresponding relative error with the temperature range 150 ± 3 °C is less than 2%. In contrast, the sensitivity measurement results under these noises cover the intrinsic sensitivity of the vapor cell, which is between 8 fT·Hz$^{-1/2}$ and 14 fT·Hz$^{-1/2}$, rendering the vapor cell evaluation invalid. Therefore, the total relaxation rate measurement method based on the magnetic resonance experiment proposed in this work has high robustness and can evaluate a vapor cell under the disturbance of external environmental noise. We will focus on the generality of this method for vapor cells with different components.

Acknowledgment

Project supported by the National Natural Science Foundation of China (Grant Nos. 62173020 and 62103381).

References

[1] Fan L M, Zheng Q, Kang X Y, Zhang X J and Kang C 2018 *Chin. Phys. B* **27** 060703
[2] Chen D, Zhao B Q and Zhang X 2015 *Chin. Phys. Lett.* **32** 128502
[3] Zhang S L and Cao N 2020 *Chin. Phys. B* **29** 040702
[4] Li J J, Du P C, Fu J Q, Wang X T, Zhou Q and Wang R Q 2019 *Chin. Phys. B* **28** 040703
[5] Kominis I K, Kornack T W, Allred J C and Romalis M V 2003 *Nature* **422** 596
[6] Dang H B, Maloof A C and Romalis M V 2010 *Appl. Phys. Lett.* **97** 151110
[7] Boto E, Holmes N, Leggett J, Roberts G, Shah V, Meyer S S, Munoz L D, Mullinger K J, Tierney T M, Bestmann S, Barnes G R, Bowtell R and Brookes M J 2018 *Nature* **555** 657
[8] Chi H T, Quan W, Zhang J Y, Zhao L J and Fang J C 2020 *Appl. Surf. Sci.* **501** 143897
[9] Wang X L, Ye M, Lu F, Mao Y K, Tian H and Li J L 2022 *Biosensors* **12** 165
[10] Kitching J 2018 *Appl. Phys. Rev.* **5** 031302
[11] Ji Y, Shang J T, Li G L, Zhang J and Zhang J F 2020 *IEEE Sens. Lett.* **4** 2500104
[12] Liu Z, Zou S, Yin K F, Zhou B Q, Ning X L and Yuan H 2022 *J. Phys. D: Appl. Phys.* **55** 285003
[13] Patton B, Ishikawa K, Jau Y Y and Happer W 2007 *Phys. Rev. Lett.* **99** 027601
[14] Perry A R, Sheng D, Krzyzewski S P, Geller S and Knappe S 2017 *Proc. SPIE* 10119, *Slow Light, Fast Light, and Opto-Atomic Precision Metrology X*, 101190V
[15] Wang Y X, Jin G, Tang J J, Zhou W Y, Han B C, Zhou B Q and Shi T 2022 *Opt. Express* **30** 336
[16] Wang Y X, Shi T, Zhou W Y, Tang J J, Zhou B Q, Jin G, Han B C and Zou S 2022 *Opt. Express* **30** 23587
[17] Sun Z Y, Fierlinger P, Han J C, Li L Y, Liu T H, Schnabel A, Stuiber S and Voigt J 2021 *IEEE Trans. Ind. Electron.* **68** 5385
[18] Xing B Z, Lu J X, Sun C, Yu T T, Wu Y, Gao Y N and Han B C 2022 *Opt. Express* **30** 3854
[19] Jia Y C, Liu Z C, Chai Z, Liang X Y and Wu W F 2021 *IEEE Trans. Instrum. Meas.* **70** 7005409
[20] Yan Y G, Liu G, Lin H X, Yin K F, Wang K and Lu J X 2021 *Chin. Opt. Lett.* **19** 121407
[21] Zhao T, Liu Y, Wei K, Xie H T, Mu T J, Fang X J, Xu Z T and Zhai Y Y 2022 *J. Phys. D: Appl. Phys.* **55** 165103
[22] Liu F, Wu J Q and Quan W 2022 *Rev. Sci. Instrum.* **93** 015102
[23] Lu F, Lu J X, Li B, Yan Y G, Zhang S W, Yin K F, Ye M and Han B C 2022 *IEEE Trans. Instrum. Meas.* **71** 1501210
[24] Zou S, Zhang H, Chen X Y and Fang J C 2022 *Measurement* **187** 110338
[25] Kamada K, Ito Y, Ichihara S, Mizutani N and Kobayashi T 2015 *Opt. Express* **23** 6976
[26] Lu J X, Qian Z, Fang J C and Quan W 2015 *Rev. Sci. Instrum.* **86** 083103
[27] Fang J C and Qin J 2012 *Rev. Sci. Instrum.* **83** 103104
[28] Ji A C, Xie X C, Liu W M 2007 *Phys. Rev. Lett.* **99** 183602
[29] Tang J J, Liu Y, Wang Y X, Zhou B Q, Han B C, Zhai Y Y and Liu G 2022 *Appl. Phys. Lett.* **120** 084001
[30] Liu X J, Ding M, Li Y, Hu Y H, Jin W and Fang J C 2018 *Chin. Phys. B* **27** 073201
[31] Savukov I M and Romalis M V 2005 *Phys. Rev. A* **71** 023405
[32] Lu J X, Qian Z and Fang J C 2015 *Rev. Sci. Instrum.* **86** 043104
[33] Romalis M V, Miron E and Cates G D 1997 *Phys. Rev. A* **56** 4569
[34] Rotondaro M D and Perram G P 1997 *J. Quant. Spectrosc. Radiat. Transfer* **57** 497